Ultramicroscopy 234 (2022) 113456

Contents lists available at ScienceDirect

Ultramicroscopy

journal homepage: www.elsevier.com/locate/ultramic

Unitary two-state quantum operators realized by quadrupole fields in the electron microscope

Stefan Löffler

University Service Centre for Transmission Electron Microscopy, TU Wien, Wiedner Hauptstraße 8-10/E057-02, 1040, Wien, Austria

ARTICLE INFO

Keywords:
Electron microscopy
Unitary operator
Qubit
Vortex beam

ABSTRACT

In this work, a novel method for using a set of electromagnetic quadrupole fields is presented to implement arbitrary unitary operators on a two-state quantum system of electrons. In addition to analytical derivations of the required quadrupole and beam settings which allow an easy direct implementation, numerical simulations of realistic scenarios show the feasibility of the proposed setup. This is expected to pave the way not only for new measurement schemes in electron microscopy and related fields but even one day for the implementation of quantum computing in the electron microscope.

1. Introduction

Unitary operators play a vital role across quantum mechanics and related fields as they model transformations between orthonormal bases. In transmission electron microscopy (TEM), the best-known such transformation is the Fourier transform which relates position space and reciprocal space and can be realized easily using a standard, round lens [1]. Going from position space representation into reciprocal space representation allows the efficient determination of crystal structures and orientations with better accuracy and signal-to-noise ratio (SNR) than, e.g., when using high-resolution TEM images acquired in imaging mode. One primary reason for this is the fact that all electrons carrying a certain information — e.g., about the lattice plane distance — are focused in one spot in reciprocal space, while being distributed over the whole micrograph in position space. Thus, measuring a few electrons in a specific reciprocal space point already gives quantifiable information about the lattice plane spacing, whereas measuring the same (low) number of electrons in a position space image will just give a few counts scattered over the entire field of view.

Another example of a unitary transformation is the use of a quadratic phase plate for measuring the orbital angular momentum (OAM) of a pure electron vortex beam [2]. Recently, an effective basis transformation was also employed to measure the OAM spectrum of an electron beam by means of a log-polar transformation [3]. In that instance, too, a setup was found that transformed different OAM components in such a way that they showed up in unique measurement channels — similar to diffraction spots —, rather than producing small variations on an otherwise fairly large signal.

The idea of having a direct one-to-one correspondence between the intensity in a channel and the sought information is closely related to the concept of sparsity commonly found in compressed sensing applications (see, e.g., [4–6] and references therein) and blind source separation (see, e.g., [7]). These methods, however, are post-processing techniques that in many cases require prior knowledge about the measured quantity. Above all else, however, their outcome strongly depends on the quality of the measured data, which in turn is heavily influenced by various noise sources, including shot noise and different electronic noise contributions in the read-out and processing components. However, unitary operators do not suffer from this problem.

Unitary operators can be applied directly to a (quantum) system *before* a measurement, thus allowing the measurement to be performed in a basis with optimal signal sparsity and SNR. The key requirement for this, however, is to find a way to perform the necessary unitary transformations directly in the instrument.

It must be emphasized that the use of unitary operators is not limited to the measurement process. It can also be used for shaping the beam. For example, a specific transformation has been used for producing electron vortex beams [8–10].

In this work, a setup is described that allows to realize arbitrary unitary operators on a two-state quantum system in a TEM. Two-state quantum systems are of particular importance as they model qubits, the building blocks of quantum computers. Such free electron qubits [11] would have many beneficial properties, from easy manipulation down to the sub-Ångstrom regime in a TEM to well-established measurement devices to very weak interaction with the environment to (in principle) easy storage, e.g. in a magnetic storage ring. Additionally, interactions

E-mail address: stefan.loeffler@tuwien.ac.at.

https://doi.org/10.1016/j.ultramic.2021.113456
Received 10 September 2021; Received in revised form 26 November 2021; Accepted 5 December 2021
Available online 8 January 2022

with photons or quantum dots or other physical qubit implementations can be triggered easily [12]. Moreover, recent advances also outline potential roads towards scaling this from one to several qubits [13–16].

Apart from the fundamental research aspects, the two-state system acts as an important model for the future development of setups for unitary operators on higher-dimensional systems. Such developments could give rise to new optimized measuring schemes with improved SNR as outlined above which would be of great practical importance in electron microscopy.

2. Theory

Here, we use the vector space $\mathcal{V}$ spanned by the two orthonormal states $|0\rangle, |1\rangle$ given in position representation as

$$\begin{aligned}\langle\vec{r}|0\rangle &= HG_{1,0}(\vec{r}) \propto x \cdot \mathrm{e}^{-\frac{r^2}{w(z)^2}} \cdot \mathrm{e}^{-\frac{\mathrm{i}kr^2}{2R(z)}} \cdot \mathrm{e}^{\mathrm{i}\gamma(z)} \\ \langle\vec{r}|1\rangle &= HG_{0,1}(\vec{r}) \propto y \cdot \mathrm{e}^{-\frac{r^2}{w(z)^2}} \cdot \mathrm{e}^{-\frac{\mathrm{i}kr^2}{2R(z)}} \cdot \mathrm{e}^{\mathrm{i}\gamma(z)},\end{aligned} \tag{1}$$

where $HG_{n,m}$ denotes the Hermite-Gaussian mode of order (n, m) [9,17,18], $w(z) = w_0\sqrt{1+(z/z_R)^2}$ is the propagation-dependent beam size with the minimal beam waist $w_0 = \sqrt{2z_R/k}$ and the Rayleigh range z_R, k is the wave number, $R(z) = z(1+(z_R/z)^2)$ is the curvature radius, and $\gamma(z) = \arctan(z/z_R)$ is the Gouy phase. Due to their primary orientation, $|0\rangle$ will be referred to as "horizontal" and $|1\rangle$ will be referred to as "vertical" in the following.

Apart from a global phase factor, all normalized states $|\psi\rangle \in \mathcal{V}$ can be written as

$$|\psi\rangle = \cos(\theta/2)|0\rangle + \sin(\theta/2)\mathrm{e}^{\mathrm{i}\varphi}|1\rangle \tag{2}$$

with $\theta \in [0, \pi], \varphi \in [0, 2\pi)$. Thus, all such states lie on the Bloch sphere (with the polar angle θ and the azimuthal angle φ) as depicted in Fig. 1. Unitary operators are simply those changing θ and φ, i.e. rotations on the sphere. Following the scheme of (extrinsic) Euler angles, it is well-known that any arbitrary rotation can be decomposed into three successive rotations around cardinal axes, e.g. in the order x–z–x.

From Fig. 1 it can be seen that rotations around x correspond to changing θ. As is evident from Eqs. (1) and (2), such an operation in the chosen basis corresponds to a rotation of the coordinate system in the plane perpendicular to the optical axis by an angle of $\delta\theta/2$, i.e. $\vec{r} \mapsto \hat{R}\vec{r}$, which can be realized in two ways: either one rotates the experimental setup (electro-magnetic fields, image, sample, etc.), which may even be achievable in post-processing in some cases, or one uses the well-known Larmor rotation [19–23] in the magnetic field of round lenses ubiquitous in electron microscopy. Note that the first approach, i.e., rotating the electro-magnetic fields, is easy in the case of quadrupole fields as those can be rotated simply by changing the excitation of the four poles.

The second ingredient to realizing arbitrary unitary operators on $\mathcal{V}$ is the ability to change φ, i.e., rotations around z in Fig. 1. From Eq. (2), it is evident that this corresponds to a relative phase shift between the two basis states. Here, a scheme for creating electron vortex beams (EVB) can be extended upon: the so-called "mode conversion" [8–10], which is based on the idea of the optical mode converter [17] and uses a set of two quadrupole lenses to convert a $HG_{1,1}$ beam into a $LG_{0,\pm1}$ beam by means of the specific phase shift of $\delta\varphi = \pm\pi/2$. Here, this approach will be generalized to arbitrary phase shifts.

Fig. 2 shows the principle setup of a relative phase shifter, consisting of two quadrupole lenses. The first quadrupole (QP1) produces an astigmatic beam from an incident round beam. The beam is focused in one direction (say, horizontally) before the second quadrupole (QP2), while it is defocused in the orthogonal direction. Due to this difference, the horizontal and vertical components (corresponding to the basis states $|0\rangle$ and $|1\rangle$, respectively) acquire different Gouy phase shifts, thus resulting in a relative phase shift by the time they reach QP2. QP2 then has to be set up to compensate the action of QP1 and produce a non-astigmatic beam again.

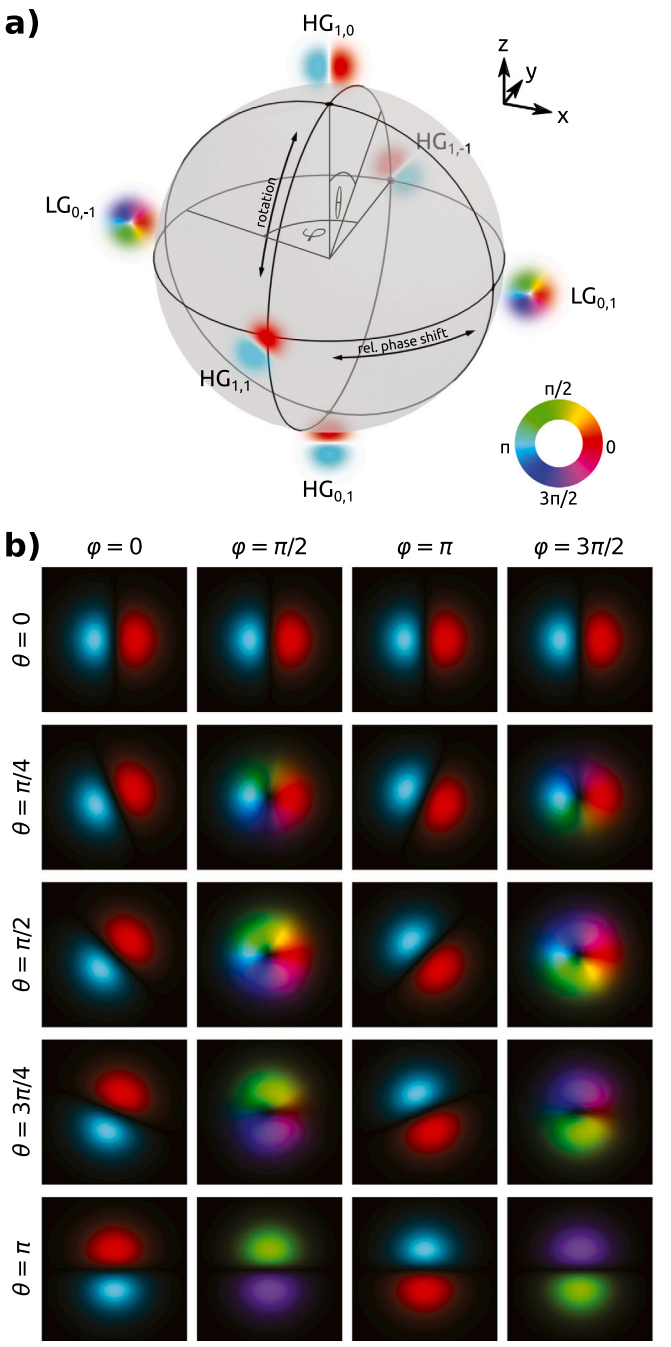

Fig. 1. (a) Schematic of the Bloch sphere for the vector space described in the text. (b) Selected states for various values of θ, φ according to Eq. (2). For all depicted states, intensity represents amplitude and color represents phase as indicated in the color wheel inset.

To model the propagation of the beam through the QP lens setup, it is beneficial to introduce the complex beam parameter $q(z) = z - z_0 + \mathrm{i}z_R$ for the two components, where z_0 is the position of the component's focus [18]. Without loss of generality, $z_0 = 0$ will be assumed in the following. The complex beam parameter completely defines a Gaussian beam and allows to calculate all its properties such as

$$w(z) = \sqrt{\frac{2|q|^2}{k\Im[q]}} \qquad R(z) = \frac{|q|^2}{\Re[q]} \qquad \gamma(z) = -\arg[\mathrm{i}q]\,. \tag{3}$$

Additionally, both the propagation and the action of a lens can be modeled easily. Propagation over a distance δz transforms $q \mapsto q + \delta z$,

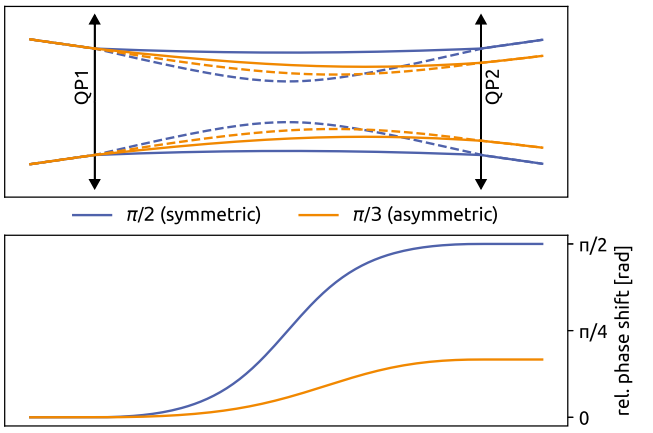

Fig. 2. Sketch of a relative phase shifter consisting of two quadrupoles (QP1, QP2). Two different settings leading to different phase shifts are shown (blue and orange). The top panel shows the horizontal (full lines) and vertical (dashed lines) beam diameters. The bottom panel shows the relative phase shift. In the shown scenario, the incident beam size was fixed.

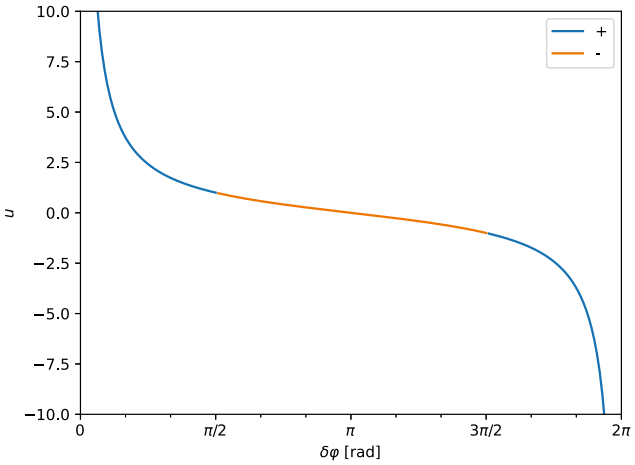

Fig. 3. Plot of u over $\delta\varphi$. The color represents the branch (the + or − variant of Eq. (6)) that produces the correct result.

while a lens with focal length f transforms $q \mapsto 1/(1/q - 1/f)$. A QP can then be modeled as a lens with focal length f for one component (e.g., the horizontal one) and $-f$ for the other component (e.g., the vertical one) [24].

The mode matching condition, i.e., the condition that the beam is round and non-astigmatic after QP2, results in the two conditions $w_h(z_2) = w_v(z_2)$ and $R_h(z_2) = R_v(z_2)$, where the subscripts h, v denote the horizontal and vertical components, respectively, and z_2 is the position of QP2. The first of the two conditions ensures that the beam is round at QP2, while the second condition ensures that it stays round even when propagating further after QP2 (i.e, it is non-astigmatic). It is easily seen that mode matching is achieved if $q_h(z_2) = q_v(z_2)$ [9]. A lengthy but straight-forward calculation (see Appendix) shows that for two quadrupoles with focal lengths f_1, f_2 at a distance d, this can be achieved for an incident beam with

$$q_{\text{in}} = -d\, f_1 \frac{f_1 + \mathrm{i}du}{f_1^2 + d^2u^2} \quad \text{with} \quad u = -\operatorname{sgn}[f_1]\sqrt{\frac{f_1 f_2}{d^2} - 1}, \tag{4}$$

with a relative phase shift of

$$\delta\varphi = \arctan\left[\frac{2u}{u^2 - 1}\right]. \tag{5}$$

Solving for u gives

$$u = \frac{1 \pm \sqrt{1 + \tan^2\delta\varphi}}{\tan\delta\varphi}. \tag{6}$$

This allows to calculate u for any given relative phase shift $\delta\varphi$, where the sign has to be chosen appropriately for the quadrant in the x-y-plane in which points with polar angle $\delta\varphi$ lie (corresponding to the normalized point $\frac{1}{u^2+1}(u^2 - 1, 2u)$ according to Eq. (5); see also Appendix). As shown in Fig. 3, for $\delta\varphi \in [0, \pi/2] \cup [3\pi/2, 2\pi]$ the + branch of Eq. (6) has to be taken whereas for $\delta\varphi \in (\pi/2, 3\pi/2)$ the − branch has to be taken. Knowing u in turn fixes the relation between f_1 and f_2 according to Eq. (4).

As a first example, consider $\delta\varphi = \pi/6$. $\tan\delta\varphi = 1/\sqrt{3} \approx 0.577$, resulting in the two solutions $u = \sqrt{3} + 2 \approx 3.732$ and $u = \sqrt{3} - 2 \approx -0.268$. The first solution corresponds to the (correct) point $(0.866, 0.5)$ in the first quadrant, while the second solution corresponds to the (incorrect) point $(-0.866, -0.5)$ in the third quadrant. Therefore, in this case, $u = \sqrt{3} + 2$ is the correct solution. Since u is positive, f_1 must be negative (diverging the horizontal component). This is also seen in Fig. 2.

As a second example, consider the phase shift $\delta\varphi = -2\pi/3$. $\tan\delta\varphi = \sqrt{3} \approx 1.732$, resulting in the two solutions $u = \sqrt{3} \approx 1.732$ and $u = -1/\sqrt{3} \approx -0.577$. The first solution corresponds to the (incorrect) point $(0.5, 0.866)$ in the first quadrant, while the second solution corresponds to the (correct) point $(-0.5, -0.866)$ in the third quadrant. Therefore, in this case, $u = -1/\sqrt{3}$ is the correct solution. Since u is negative, f_1 must be positive (converging the horizontal component).

Several distinct values require special attention. These are $\delta\varphi \in \{0, \pm\pi/2, \pi\}$. For 0 and π, Eq. (6) is indeterminate. Taking the limits of $\delta\varphi \to 0$ and $\delta\varphi \to \pi$, gives the values 0 and $\pm\infty$. For $u = 0$, Eq. (4) gives $f_1 f_2 = d^2$ and $q_{\text{in}} = -d$, meaning a negligible small Rayleigh range and diverging beam size. This corresponds to the geometrical limit, i.e. a very large beam (compared to its waist size) far from its focus (compared to the Rayleigh range). One component goes through focus while the other one does not, resulting in a relative phase shift of π in the far field. $u = \pm\infty$, on the other hand, corresponds to infinite focal lengths, i.e., switched off quadrupoles and no relative phase shift.

$\delta\varphi = \pm\pi/2$ is the special case used for vortex creation. For these values, Eq. (6) is also indeterminate. Taking the limits results in the values $u = \pm 1$. Taking the corresponding limits in Eq. (5) shows that $u = 1$ corresponds to $\delta\varphi = \pi/2$ and $u = -1$ corresponds to $\delta\varphi = -\pi/2$. In both cases, Eq. (4) gives the well-known condition $f_1 f_2 = 2d^2$ for vortex creation [9].

Another lengthy but straight-forward calculations shows that the beam parameter of the outgoing beam (directly after QP2) reads

$$q_{\text{out}} = -d\, f_2 \frac{-f_2 + \mathrm{i}du}{f_2^2 + d^2u^2}. \tag{7}$$

Noteworthy properties of the incident and the outgoing beam are

$$\begin{aligned} |q_{\text{in}}|^2 &= \frac{d^2 f_1^2}{f_1^2 + d^2u^2} \qquad w_{\text{in}} = \sqrt{-\frac{2f_1}{ku}} \qquad R_{\text{in}} = -d \\ |q_{\text{out}}|^2 &= \frac{d^2 f_2^2}{f_2^2 + d^2u^2} \qquad w_{\text{out}} = \sqrt{-\frac{2f_2}{ku}} \qquad R_{\text{out}} = d. \end{aligned} \tag{8}$$

With these values, it is possible to express f_1 as a function of w_{in} and u, thus yielding the following alternative form of the incident beam parameter

$$q_{\text{in}} = \frac{-dk^2 w_{\text{in}}^4 + 2\mathrm{i}d^2 k w_{\text{in}}^2}{k^2 w_{\text{in}}^4 + 4d^2} \tag{9}$$

with

$$f_1 = -\frac{kuw_{\text{in}}^2}{2} \quad \text{and} \quad f_2 = \frac{d^2}{f_1}(u^2 + 1) \tag{10}$$

To sum up, for given $\delta\varphi$, the dimensionless parameter u is uniquely determined and Eq. (10) gives the QP settings required to obtain $\delta\varphi$ for a given incident beam (with size w_{in} and curvature $-d$).

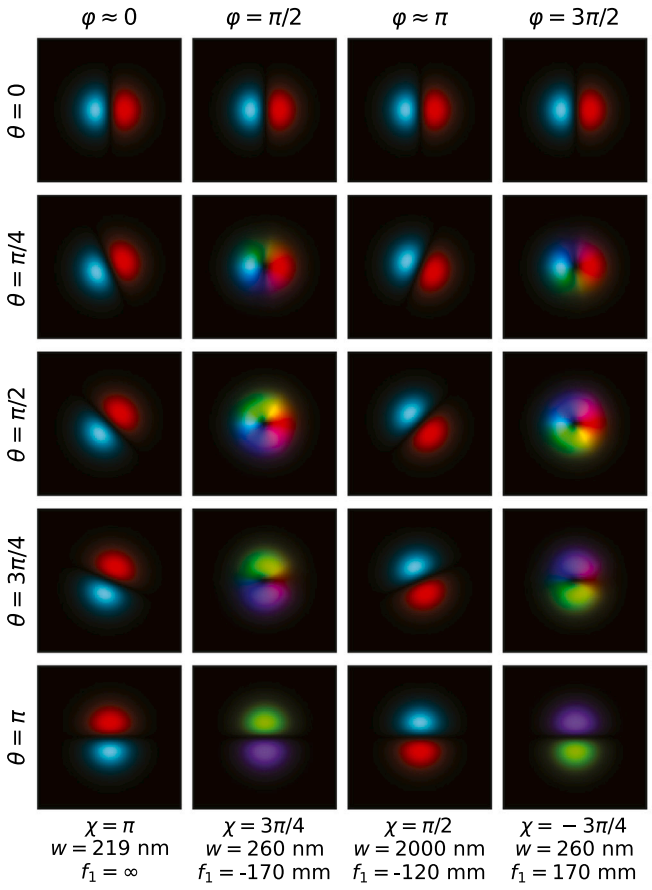

Fig. 4. Simulations of the phase shifter setup for the same values of θ, φ as in Fig. 1. In all cases, the incident beam was a $HG_{1,0}$ beam rotated by $\theta/2$. For each φ, the incident beam size w, the QP1 focal length f_1, and the global phase compensation χ are indicated. For illustration purposes, a symmetric setup with $w_{in} = w_{out}$ and $f_1 = f_2$ was used. For $f_1 = \infty$, a numerical value of 1 km was used. Amplitude and phase are shown as in Fig. 1.

3. Simulations

To corroborate the theoretical results, numerical simulations were performed using the *virTUal TEM* software package [9]. All optical elements were modeled as effective phase plates (i.e., thin elements) and the propagation was performed in paraxial approximation using a Fourier-space Fresnel propagator (owing to the small beam diameters and convergence angles). All simulations were performed for an incident $HG_{1,0}$ beam rotated by $\theta/2$ with an energy of 200 keV using a setup as shown in Fig. 2. For simulation simplicity, a symmetric setup (i.e., $f_1 = f_2$) was chosen in all cases. To achieve the required curvature radius of the incident beam, an initially non-diffracting beam was transformed into a convergent beam using a round transfer lens before QP1. For clarity, a matching round lens after QP2 was included to flatten the phase front to ease comparability. The two QPs had a spacing of $d = 120$ mm.

For numerical reasons, both the focal lengths and the beam sizes were bounded. The focal length was limited to $|f_1| \leq 1$ km, resulting in a minimal achievable phase shift of $\delta\varphi \approx 0.24$ mrad, while the beam size was limited to $w_{in} \leq 2$ µm resulting in phase shifts between 3.09 rad and 3.19 rad being unachievable with a single phase shifter setup.

The results are summarized in Fig. 4. A comparison to Fig. 1 shows perfect agreement. It should be noted that in all cases except $\varphi = 0$, the beam acquired a global phase χ as indicated in the figure. This stems from the propagation distance between the QPs, similar to the optical path length in light optics. As the global phase is inconsequential in this work (and can be compensated for by physical flight paths, lens systems, or temporarily changing the speed of the electrons), it is removed from the images in Fig. 4 for better comparability.

In terms of practical applicability, the chosen parameters, while not specific to any particular instrument, are in a realistic order of magnitude range. Also the beam sizes of a few hundred nanometers are readily achievable in a TEM. As far as the incident beam is concerned, no perfect Gaussian beams have been produced to date, but sufficiently close approximations are possible [2,8,9,21].

4. Discussion & outlook

Some properties of this setup are worth emphasizing. First, in order to achieve mode matching, the incident beam must have a curvature at QP1 of $-d$, meaning that in the geometric limit (for large beams), it is focused at QP2 (although for small beams, the focus will be in front of QP2). This can easily be achieved by a transfer lens before the quadrupoles.

Second, focal lengths f_1, f_2 (and therefore the beam sizes w_{in}, w_{out}) are coupled by the phase shift. Thus, while it is possible for a given phase shift to choose either the incident or the outgoing beam size, it is not possible to choose both at the same time. Again, this can be compensated if needed by a transfer lens system.

Third, phase shifts close to 0 lead to a very large magnitude of u and, hence, of the focal lengths. Such long focal lengths typically require very small excitations of the QPs which may not be controllable with suitable accuracy. This can be worked around by a two-step process: to achieve a small relative phase shift ε, first shift by a large α and then by $-\alpha + \varepsilon$. Similarly, phase shifts around π lead to very small u and therefore require very short focal lengths (or very large beam sizes). This, too, can be worked around by a two-step process: to achieve a phase shift of $\alpha \sim \pi$, one can instead perform two shifts by $\alpha/2$.

The setup in this work, i.e. two quadrupoles acting on a specific two-state quantum system, is, of course, a simple model system for studying unitary transformations. One big advantage of this system is that it can readily be investigated in existing TEMs [10] without the need for any changes to the instrument or the development of custom electron-optical elements. In the future, however, it will certainly be beneficial to expand this concept to other systems, in particular higher-dimensional quantum systems. On the one hand, this will facilitate enhanced measurement schemes with improved SNR for common microscopy tasks (which are usually not confined to a two-state quantum system). On the other hand, this will allow for the handling of n-state qudits (as opposed to 2-state qubits). Such a system will likely have to rely on advanced — and probably adaptive — methods for phase manipulation, such as programmable phase manipulators [13,25,26] akin to spatial light modulators (SLMs) in optics.

Performing quantum computations in an electron microscope in the future will require the realization of so-called universal quantum gates [27] — similar to universal logic gates such as NAND in conventional computing. One key ingredient to this is unitary transformations (or so-called one-qubit gates) which can arbitrarily change the state of a single qubit as presented in this paper. The other ingredient is at least one two-qubit gate such as CNOT. It can be shown that such a gate is entangling [27], i.e. it creates entanglement between previously unentangled systems. One common way this is achieved in electron microscopy is scattering [28,29]. However, it is still an open question how scattering experiments could be designed — e.g. using wave front shaping of the electron beams before and after scattering — such that most electrons scatter into an (entangled) state inside the vector space spanned by the chosen basis vectors ($HG_{1,0}$ and $HG_{0,1}$ in the case discussed in this work).

Additionally, in a quantum computing scheme, one will eventually want to increase the number of quantum gates. As far as pairs of quadrupoles (and higher-order multipoles that can be driven to act

as quadrupoles) are concerned, current TEMs are limited to at most a handful, spread between the condensor/probe corrector system, the imaging lenses/image corrector system, and potentially an imaging filter. Similarly, there is a very limited number of (aperture) planes in which programmable phase manipulators could be inserted by default. Thus, large-scale quantum computation applications will require additional custom elements added to a TEM or even a complete custom instrument. However, for the time being, many open questions and tasks remain that can easily be investigated with the handful of elements at our disposal in a general-purpose TEM.

5. Conclusions

In this work, a novel concept for using mode converters in the TEM was presented that allows the realization of arbitrary unitary operators on a two-state quantum system. This paves the way for the realization of higher-dimensional unitary operators, which in turn will open entirely new possibilities for electron microscopy and all fields it is applied in, from physics to material science and chemistry to biology. Instead of post-processing data and looking for tiny signals in a huge, noisy background, the realization of unitary operators will allow much more efficient experiments by enabling scientists to devise measurement schemes where the electron beam is quantum-mechanically transformed into a basis in which the sought information can be read out directly. Moreover, together with the recent progress in understanding entanglement of free electrons, this work may well contribute one day to performing quantum computations in the electron microscope.

Declaration of competing interest

The authors declare that they have no known competing financial interests or personal relationships that could have appeared to influence the work reported in this paper.

Acknowledgments

S.L. acknowledges fruitful discussions with Peter Schattschneider and financial support by the Austrian Science Fund (FWF) under grant nrs. I4309-N36 and P29687-N36 and by TU Wien Bibliothek through its Open Access Funding Programme.

Appendix. Derivation of the mode matching condition and the phase shift

In this section, the matrix transfer method [18,24] is heavily used to derive the general mode-matching criteria for Hermite-Gaussian waves in a two-quadrupole setup. For a closely related treatment in a charged-particle formalism, see e.g. [24].

The effect of lenses ($\boldsymbol{L}$) and free space ($\boldsymbol{T}$) is modeled by matrices

$$\boldsymbol{L}(f) = \begin{pmatrix} 1 & 0 \\ -\frac{1}{f} & 1 \end{pmatrix} \qquad \boldsymbol{T}(d) = \begin{pmatrix} 1 & d \\ 0 & 1 \end{pmatrix} \tag{A.1}$$

where f is the lens' focal length and d is the distance the beam propagates through free space. An optical system of several components can be described by the product of the individual component matrices. Assuming a system described by

$$\boldsymbol{M} = \begin{pmatrix} A & B \\ C & D \end{pmatrix}, \tag{A.2}$$

a complex beam parameter q_{in} is transformed according to

$$q_{\mathrm{out}} = \frac{Aq_{\mathrm{in}} + B}{Cq_{\mathrm{in}} + D}. \tag{A.3}$$

Mathematically, this corresponds to a projective transform which can be modeled in matrix notation by

$$\vec{q}_{\mathrm{out}} = \boldsymbol{M} \cdot \begin{pmatrix} q_{\mathrm{in}} \\ 1 \end{pmatrix} = \boldsymbol{M} \cdot \vec{q}_{\mathrm{in}} \tag{A.4}$$

if all vectors that only differ by a non-zero scalar factor are treated as equivalent.

The two quadrupole setup discussed in this work can therefore be modeled by two matrices

$$\begin{aligned} \boldsymbol{M}_h &= \boldsymbol{L}(f_2) \cdot \boldsymbol{T}(d) \cdot \boldsymbol{L}(f_1) \\ \boldsymbol{M}_v &= \boldsymbol{L}(-f_2) \cdot \boldsymbol{T}(d) \cdot \boldsymbol{L}(-f_1) \end{aligned} \tag{A.5}$$

owing to the fact that quadrupoles act differently on horizontal and vertical components. The mode matching condition thus becomes

$$\boldsymbol{M}_h \vec{q}_{\mathrm{in}} \propto \boldsymbol{M}_v \vec{q}_{\mathrm{in}} \tag{A.6}$$

or, equivalently,

$$\boldsymbol{M}_v^{-1} \boldsymbol{M}_h \vec{q}_{\mathrm{in}} = \lambda \vec{q}_{\mathrm{in}} \tag{A.7}$$

where the proportionality comes from the equivalence of vectors that are scalar multiples of one another. Thus, finding an incident beam that is mode matched at the output is equivalent to finding an eigenvector of Eq. (A.7). Note that the eigenvectors of a matrix of the form given in Eq. (A.2) — given $C \neq 0$ — can be directly derived as

$$\boldsymbol{M} \begin{pmatrix} q \\ 1 \end{pmatrix} = \begin{pmatrix} Aq + B \\ Cq + D \end{pmatrix} = \begin{pmatrix} \lambda q \\ \lambda \end{pmatrix} = \lambda \begin{pmatrix} q \\ 1 \end{pmatrix} \tag{A.8}$$

$$Cq^2 + (D - A)q - B = 0 \tag{A.9}$$

$$q = \frac{A - D \pm \sqrt{(A - D)^2 + 4BC}}{2C}. \tag{A.10}$$

In the present case, the relevant matrix reads

$$\boldsymbol{M}_v^{-1} \boldsymbol{M}_h = \frac{1}{f_1^2 f_2^2} \begin{pmatrix} f_1^2 f_2^2 + 2 f_1 f_2 d(f_1 - d) & 2 f_1^2 f_2 d^2 \\ 2 f_2 d^2 - 2 f_1 f_2 (f_1 + f_2) & f_1^2 f_2^2 - 2 f_1 f_2 d(f_1 + d) \end{pmatrix} \tag{A.11}$$

and thus

$$q_{\mathrm{in}} = \frac{f_1^2 d \pm |f_1| \operatorname{sgn}[f_2] d \sqrt{d^2 - f_1 f_2}}{d^2 - f_1^2 - f_1 f_2}. \tag{A.12}$$

Note that only one of the two solutions results in a sensible Rayleigh range (i.e. strictly positive imaginary part) and only if $f_1 f_2 > d^2$. Thus, it makes sense to rewrite the expression as

$$q_{\mathrm{in}} = \frac{-d f_1^2 + \mathrm{i} d |f_1| \sqrt{f_1 f_2 - d^2}}{f_1^2 + f_1 f_2 - d^2}. \tag{A.13}$$

This is identical to Eq. (4). For future reference, note that

$$|q_{\mathrm{in}}|^2 = \frac{d^2 f_1^2}{f_1^2 + f_1 f_2 - d^2}. \tag{A.14}$$

To calculate the relative phase shift, one needs to calculate the beam parameters directly after QP1 ($q_{1,h}, q_{1,v}$) at z_1 and directly before QP2 ($q_{2,h}, q_{2,v}$) at z_2. Direct calculation yields the expressions

$$\begin{aligned} q_{1,h} &= \frac{q_{\mathrm{in}} f_1}{f_1 - q_{\mathrm{in}}} & q_{2,h} &= \frac{d f_1 + (f_1 - d) q_{\mathrm{in}}}{f_1 - q_{\mathrm{in}}} \\ q_{1,v} &= \frac{q_{\mathrm{in}} f_1}{f_1 + q_{\mathrm{in}}} & q_{2,v} &= \frac{d f_1 + (f_1 + d) q_{\mathrm{in}}}{f_1 + q_{\mathrm{in}}}. \end{aligned} \tag{A.15}$$

The relative phase shift is thus

$$\begin{aligned} \delta\varphi &= -\arg[\mathrm{i} q_{2,v}] + \arg[\mathrm{i} q_{1,v}] + \arg[\mathrm{i} q_{2,h}] - \arg[\mathrm{i} q_{1,h}] \\ &= \arg\left[\frac{q_{1,v} q_{2,h}}{q_{1,h} q_{2,v}}\right] = \arg\left[q_{1,h}^* q_{1,v} q_{2,h} q_{2,v}^*\right] \\ &= \arg\left[(d f_1 + (f_1 - d) q_{\mathrm{in}})(d f_1 + (f_1 + d) q_{\mathrm{in}})^*\right] \\ &= \arg\left[d^2 f_1^2 + (f_1^2 - d^2)|q_{\mathrm{in}}|^2 + 2 d f_1^2 \Re[q_{\mathrm{in}}] - 2\mathrm{i} d^2 f_1 \Im[q_{\mathrm{in}}]\right] \end{aligned}$$

$$= \arctan\left(\frac{-2d^2 f_1 \Im[q_{\text{in}}]}{d^2 f_1^2 + (f_1^2 - d^2)|q_{\text{in}}|^2 + 2d f_1^2 \Re[q_{\text{in}}]}\right) \tag{A.16}$$

where the fact that a positive (real) factor does not change the argument of a complex number was used. Note that it is important to keep the minus sign in the numerator (rather than moving it to the denominator or in front of the fraction) to ensure the correct quadrant can be determined (as arctan is unique only up to an integer multiple of π). Applied to the specific case of Eq. (A.13) gives

$$\tan\delta\varphi = \frac{-2d\ \text{sgn}[f_1]\sqrt{f_1 f_2 - d^2}}{f_1 f_2 - 2d^2}. \tag{A.17}$$

By the introduction of the dimensionless parameter

$$u = -\,\text{sgn}[f_1]\sqrt{\frac{f_1 f_2}{d^2} - 1}, \tag{A.18}$$

the phase shift can be rewritten as

$$\tan\delta\varphi = \frac{2u}{u^2 - 1}. \tag{A.19}$$

which corresponds to Eq. (5).

References

[1] D.B. Williams, C.B. Carter, Transmission Electron Microscopy, Plenum Press, New York, 1996.

[2] G. Guzzinati, L. Clark, A. Béché, J. Verbeeck, Measuring the orbital angular momentum of electron beams, Phys. Rev. A 89 (2014) 025803, http://dx.doi.org/10.1103/PhysRevA.89.025803.

[3] V. Grillo, A.H. Tavabi, F. Venturi, H. Larocque, R. Balboni, G.C. Gazzadi, S. Frabboni, P.-H. Lu, E. Mafakheri, F. Bouchard, R.E. Dunin-Borkowski, R.W. Boyd, M.P.J. Lavery, M.J. Padgett, E. Karimi, Measuring the orbital angular momentum spectrum of an electron beam, Nature Commun. 8 (2017) 15536, http://dx.doi.org/10.1038/ncomms15536.

[4] Z. Saghi, D.J. Holland, R. Leary, A. Falqui, G. Bertoni, A.J. Sederman, L.F. Gladden, P.A. Midgley, Three-dimensional morphology of iron oxide nanoparticles with reactive concave surfaces, a compressed sensing-electron tomography (CS-ET) approach, Nano Lett. 11 (11) (2011) 4666–4673, http://dx.doi.org/10.1021/nl202253a.

[5] R. Huber, G. Haberfehlner, M. Holler, G. Kothleitner, K. Bredies, Total generalized variation regularization for multi-modal electron tomography, Nanoscale 11 (12) (2019) 5617–5632, http://dx.doi.org/10.1039/c8nr09058k.

[6] M. Rani, S.B. Dhok, R.B. Deshmukh, A systematic review of compressive sensing: Concepts, implementations and applications, IEEE Access 6 (2018) 4875–4894, http://dx.doi.org/10.1109/access.2018.2793851.

[7] P. Comon, C. Jutten (Eds.), Handbook of Blind Source Separation: Independent Component Analysis and Applications, ACADEMIC PR INC, 2010, URL https://www.ebook.de/de/product/9020313/pierre_comon_handbook_of_blind_source_separation_independent_component_analysis_and_applications.html.

[8] P. Schattschneider, M. Stöger-Pollach, J. Verbeeck, Novel vortex generator and mode converter for electron beams, Phys. Rev. Lett. 109 (8) (2012) 084801, http://dx.doi.org/10.1103/physrevlett.109.084801.

[9] C. Kramberger, S. Löffler, T. Schachinger, P. Hartel, J. Zach, P. Schattschneider, $\pi/2$ mode converters and vortex generators for electrons, Ultramicroscopy 204 (2019) 27–33, http://dx.doi.org/10.1016/j.ultramic.2019.05.003, arXiv:1902.05368.

[10] T. Schachinger, P. Hartel, P. Lu, S. Löffler, M. Obermair, M. Dries, D. Gerthsen, R.E. Dunin-Borkowski, P. Schattschneider, Experimental realisation of a $\pi/2$ vortex mode converter for electrons using a spherical aberration corrector, Ultramicroscopy 229 (2021) 113340, http://dx.doi.org/10.1016/j.ultramic.2021.113340, arXiv:2103.10899.

[11] O. Reinhardt, C. Mechel, M. Lynch, I. Kaminer, Free-electron qubits, 2019, arXiv:1907.10281.

[12] R. Ruimy, A. Gorlach, C. Mechel, N. Rivera, I. Kaminer, Toward atomic-resolution quantum measurements with coherently shaped free electrons, Phys. Rev. Lett. 126 (23) (2021) 233403, http://dx.doi.org/10.1103/physrevlett.126.233403.

[13] J. Verbeeck, A. Béché, K. Müller-Caspary, G. Guzzinati, M.A. Luong, M.D. Hertog, Demonstration of a 2×2 programmable phase plate for electrons, Ultramicroscopy 190 (2018) 58–65, http://dx.doi.org/10.1016/j.ultramic.2018.03.017.

[14] P. Thakkar, V.A. Guzenko, P.-H. Lu, R.E. Dunin-Borkowski, J.P. Abrahams, S. Tsujino, Fabrication of low aspect ratio three-element boersch phase shifters for voltage-controlled three electron beam interference, J. Appl. Phys. 128 (13) (2020) 134502, http://dx.doi.org/10.1063/5.0020383.

[15] P. Rosi, G.C. Gazzadi, S. Frabboni, V. Grillo, A.H. Tavabi, R.E. Dunin-Borkowski, G. Pozzi, Focused ion beam fabrication of janus bimetallic cylinders acting as drift tube zernike phase plates for electron microscopy, J. Appl. Phys. 130 (2) (2021) 024507, http://dx.doi.org/10.1063/5.0050055.

[16] A. Eberle, S. Mikula, R. Schalek, J. Lichtman, M.K. Tate, D. Zeidler, High-resolution, high-throughput imaging with a multibeam scanning electron microscope, J. Microsc. 259 (2) (2015) 114–120, http://dx.doi.org/10.1111/jmi.12224.

[17] M. Beijersbergen, L. Allen, H. van der Veen, J. Woerdman, Astigmatic laser mode converters and transfer of orbital angular momentum, Opt. Commun. 96 (1–3) (1993) 123–132, http://dx.doi.org/10.1016/0030-4018(93)90535-d.

[18] A. Yariv, Quantum Electronics, John Wiley & Sons, 1989, URL https://www.ebook.de/de/product/3635586/amnon_yariv_yariv_quantum_electronics.html.

[19] I. Ennen, S. Löffler, C. Kübel, D. Wang, A. Auge, A. Hütten, P. Schattschneider, Site-specific chirality in magnetic transitions, J. Magn. Magn. Mater. 324 (18) (2012) 2723–2726, http://dx.doi.org/10.1016/j.jmmm.2012.03.050.

[20] G. Guzzinati, P. Schattschneider, K.Y. Bliokh, F. Nori, J. Verbeeck, Observation of the larmor and gouy rotations with electron vortex beams, Phys. Rev. Lett. 110 (2013) 093601, http://dx.doi.org/10.1103/PhysRevLett.110.093601.

[21] P. Schattschneider, T. Schachinger, M. Stöger-Pollach, S. Löffler, A. Steiger-Thirsfeld, K.Y. Bliokh, F. Nori, Imaging the dynamics of free-electron landau states, Nature Commun. 5 (2014) 4586, http://dx.doi.org/10.1038/ncomms5586, arXiv:1408.1972.

[22] T. Schachinger, S. Löffler, M. Stöger-Pollach, P. Schattschneider, Peculiar rotation of electron vortex beams, Ultramicroscopy 158 (2015) 17–25, http://dx.doi.org/10.1016/j.ultramic.2015.06.004, arXiv:1703.10235.

[23] K.Y. Bliokh, P. Schattschneider, J. Verbeeck, F. Nori, Electron vortex beams in a magnetic field: A new twist on landau levels and aharonov-bohm states, Phys. Rev. X 2 (2012) 041011, http://dx.doi.org/10.1103/PhysRevX.2.041011.

[24] H. Rose, Geometrical Charged-Particle Optics, Springer-Verlag GmbH, 2013, URL https://www.ebook.de/de/product/25039540/harald_rose_geometrical_charged_particle_optics.html.

[25] G. Guzzinati, L. Clark, A. Béché, R. Juchtmans, R.V. Boxem, M. Mazilu, J. Verbeeck, Prospects for versatile phase manipulation in the tem: Beyond aberration correction, Ultramicroscopy 151 (2015) 85–93, http://dx.doi.org/10.1016/j.ultramic.2014.10.007, special Issue: 80th Birthday of Harald Rose; {PICO} 2015 – Third Conference on Frontiers of Aberration Corrected Electron Microscopy. URL http://www.sciencedirect.com/science/article/pii/S0304399114001995.

[26] G. Pozzi, V. Grillo, P.-H. Lu, A.H. Tavabi, E. Karimi, R.E. Dunin-Borkowski, Design of electrostatic phase elements for sorting the orbital angular momentum of electrons, Ultramicroscopy 208 (2020) 112861, http://dx.doi.org/10.1016/j.ultramic.2019.112861.

[27] C.P. Williams, Quantum gates, in: Texts in Computer Science, Springer London, 2011, pp. 51–122, http://dx.doi.org/10.1007/978-1-84628-887-6_2.

[28] P. Schattschneider, S. Löffler, Entanglement and decoherence in electron microscopy, Ultramicroscopy 190 (2018) 39–44, http://dx.doi.org/10.1016/j.ultramic.2018.04.007.

[29] P. Schattschneider, S. Löffler, H. Gollisch, R. Feder, Entanglement and entropy in electron–electron scattering, J. Electron Spectrosc. Relat. Phenom. 241 (2020) 146810, http://dx.doi.org/10.1016/j.elspec.2018.11.009, arXiv:1807.04694.